Direct air capture based on ionic liquids: From molecular design to process assessment

D. Hospital-Benito [a], C. Moya [a], M. Gazzani [b,c], J. Palomar [a,*]

[a] Chemical Engineering Department, Universidad Autónoma de Madrid. Francisco Tomás y Valiente 7, 28049 Madrid, Spain
[b] Copernicus Institute of Sustainable Development, Utrecht University. Princetonlaan 8a, 3584 CB Utrecht, The Netherlands
[c] Inorganic Membranes and Membrane Reactors, Sustainable Process Engineering, Chemical Engineering and Chemistry, Eindhoven University of Technology, Eindhoven, The Netherlands

ABSTRACT

Direct air capture is a key carbon dioxide removal technology to mitigate climate change and keep the global average temperature rise below 1.5–2 °C. This work addresses for the first time the use of ionic liquids for direct air capture connecting their material design by molecular simulation to process modelling. First, 26 different ionic liquids were designed through quantum chemical calculations and their isotherms were computed to identify those with a positive cyclic working capacity at conditions relevant for direct air capture. Then, the most promising ionic liquids were assessed via process simulations in Aspen Plus. A wide range of operating configurations were screened by modifying the key process variables: air velocity (1 – 3 m/s), solvent mass flow (5 – 50 t/h) and temperature (293 – 323 K), and regeneration pressure (0.1 – 1 bar) and temperature (373 – 393 K). Exergy, energy and productivity were computed to detect optimal operating conditions; moreover, a simplified economic analysis was carried out to highlight the major cost components. The direct air capture system based on $[P_{66614}][Im]$ exhibited the most exergy (5.44 – 16.73 MJ/kg) and energy (15.15 – 35.42 MJ/kg) efficiency for similar productivity (0.5 – 1.3 kg/(m^3·h)) thanks to its enhanced cyclic capacity (0.6 – 0.3 mol/kg). The minimum exergy required by $[P_{66614}][Im]$-based DAC process is slightly better than alkali scrubbing (6.21 MJ/kg) and in line with amine (5.59 MJ/kg) scrubbing. In addition, the assessed DAC process has a theoretical potential to operate in the range of 200 \$/t$_{CO2}$ under reasonable energy and plant expenses. We conclude this work providing guidelines to address future development of direct air capture technologies based on ionic liquids.

1. Introduction

Direct air capture (DAC) is a key technology to enable large scale carbon dioxide (CO_2) removal (CDR) from the atmosphere, and therefore increase the chances for a 1.5/2 °C increment in the global average temperature [1,2]. DAC extracts CO_2 from ambient air, and one of its major benefits is that it decouples the CO_2 emission point from the capture location, thus enabling to tackle the emissions from distributed sources [2,3]. Moreover, it can provide CO_2 as carbon source that does not come from fossil sources. Although DAC is a relatively new process that is in the early stages of development and commercialization, it is attracting significant attention from academics and start-up companies, thus rapidly moving from the laboratory to pilot-scale demonstration and first-of-a-kind plant operation [3,4]. Some evidences are the increasing number of publications [3], and DAC facilities operating

worldwide [5,6], and the committed/assigned funding for DAC development and deployment from public and private institutions [6,7]. In fact, the growing momentum behind DAC shall continue in future, as it is estimated that DAC has to be deployed at Gton scale by 2050 to meet the Paris Agreement goals [8,9]. While DAC will inevitably stay as an expensive technological solution – Physics teaches us so – the inherent technology modularity opens door for substantial cost reduction when deployed at scale, especially compared to the current cost range [6,10]. Large scale implementation could realistically decrease the CO_2 capture costs below 200 \$/t$_{CO2}$ but reaching the DOE target of 100 \$/ton$_{CO2}$ will be very challenging [6,8,10,11]. From this perspective, process intensification will be key to realize any substantial cost reduction.

An established approach to remove CO_2 from air at industrial scale makes use of scrubbing via aqueous alkali hydroxide, typically sodium or potassium hydroxide, which reacts with CO_2 to produce a carbonate

soluble in water [3]. This technique has evolved into a benchmark for DAC, as the Canadian-based DAC company Carbon Engineering designed a tailor-made air contactor for using a potassium hydroxide (KOH) solution to ensure an efficient air contact with the solvent [12,13]. Given that large volumes of air must be processed to extract a relevant amount of CO₂, the mass transfer resistance between air and the solvent solution must be minimized. Plans exist for the construction of a one Mt_{CO2}/year DAC facility using this process solution [14]. An early techno-economic analysis of the plant revealed a preliminary levelized cost per ton of CO₂ captured from 94 to 232 $/$t_{CO2}$ for this technology [14] yet these numbers are not independent and are not supported by the full scientific community [15]. More importantly, the major drawbacks related to the caustic recovery of the alkali hydroxide and the high temperature regeneration have not been resolved yet [16].

Alternative absorption-based DAC processes have been proposed. The use of aqueous solution of amino acids to remove CO₂ from ambient air was addressed [17], but it did not overcome the high energy demand of alkali scrubbing owing to the lower cyclic capacity of amino acid solvents [18]. Recently, the well-known amine scrubbing using monoethanolamine (MEA) was assessed as an alternative for DAC. Experimentally, aqueous MEA solutions exhibited high capture rate during a 24-hour screening of amine-based solvents for DAC [19]. Its removal efficiency can be further improved by other amines, as isophorone diamine (IPDA), thanks to a liquid–solid phase separation that overcomes the gas–liquid equilibrium limitations [20]. Regarding process simulation and economic evaluation, the conventional MEA-based absorption process was adapted for CO₂ removal from the atmosphere [21]. Moreover, the optimal air contactor unit from Carbon Engineering could potentially reduce the cost of the absorber [21], opening doors for total costs in the range of 200 $/$t_{CO2}$ [22]. On the other side, amine scrubbing still features an energy-intensive desorption, besides degradation and corrosion issues [21,23]. As a promising, alternative process route, the DAC scientific community as well as established DAC companies, (e.g., Climeworks, Global Thermostat, Carbon Capture Inc.) adopted the immobilization of amines on solid supports [24–26]. This route is currently offered commercially by several start-ups [4,5,26]. Life cycle assessments of the existing Hinwil plant operated by Climeworks, for which a cost of 600 $/$t_{CO2}$ was informed [5,11,21], revealed that substantial amount of negative CO₂ emissions can be achieved [27–29]. Metal-organic frameworks (MOFs) are another class of advanced solid materials that has been tested for DAC purposes. In fact, particularly positive energy results were achieved for MIL-101(cr)-PEI-800 and mmen-Mg2(dobpdc) [30]. Very low total costs (46 – 91 $/$t_{CO2}$) were also theoretically computed for similar sorbents [31].

In the quest for new materials to improve DAC technologies [5], ionic liquids (ILs) have hardly be considered as promising candidates [32–34]. ILs exhibit good performance in CO₂ capture, mainly because of the good stability, the low volatility, and the large possible designs, besides both high CO₂ solubility and selectivity [35]. ILs capable of reacting with CO₂ to chemically absorb it are the most promising for CO₂ capture nowadays [36]. In this sense, a 1:1 reaction mechanism was demonstrated to be essential to achieve a high absorption potential and analyzed in detail in relevant investigations [37–39]. With respect to DAC, the first IL-based examples for this purpose were developed on a laboratory scale; this used solid polymeric ILs [32] and ILs derived from waste amino acids [33]. In the former, a 1:2 CO₂:IL molar capture ratio was achieved, showing that ILs could be adapted and designed to capture CO₂ from ambient air. Similarly, literature reviews highlight the challenges to address for the application of ILs as DAC alternative: chemisorption of CO₂ is likely mandatory, energy efficiency depends on the optimum balance between CO₂ uptake capacity and reaction enthalpy, and high thermal stability -to enable the cyclic absorption/desorption process- and low viscosity -to avoid severe absorption kinetics problems as demonstrated on conventional post-combustion capture- are required [34]. In this context, Aprotic N-Heterocyclic Anion-based ionic liquids (AHA-ILs) are promising candidates for DAC

application due to their high thermal stability, 1:1 reaction stoichiometry, tunable molecular structure, which can be conveniently modified to match the enthalpy of reaction, and relatively low viscosity, which does not increase after reacting with CO₂ [38,39]. Moreover, they exhibited promising results on post-combustion capture over other ILs families [40–43], and their absorption capacity would not be adversely affected by the water present in the ambient air [44]. However, detailed process studies have not been performed yet to evaluate the feasibility of using AHA-ILs for direct air capture.

With this work, we aim at addressing this research gap by carrying out a detailed process evaluation and optimization of DAC processes based on ILs. We do this by bridging molecular design of new ILs to their process performance evaluation for DAC application. First, 26 different AHA-ILs were designed by DFT/COSMO-RS method [45,46]. Their CO₂ isotherms were predicted, and used to estimate the cyclic working capacity, thus identifying the suitable ILs for DAC. Next, advanced rate-based process modeling in Aspen Plus was used to evaluate the selected ILs in terms of productivity and exergy (and energy) demand. To this end, we adopted the design of the absorption unit based on Carbon Engineering air contactor [22]. Multiple configurations were tested by changing air velocity (1 – 3 m/s), IL mass flow (5 – 50 t/h) and temperature (293 – 323 K), and desorption pressure (0.1 – 1 bar) and temperature (373 – 393 K). In total, a few thousand cases were simulated. The combination of optimal minimum-exergy and maximum-productivity operational points were identified and represented in Pareto fronts. The impact of the IL viscosity on the results, which is notoriously the main issue associated to ILs, was studied. Finally, the exergy and productivity results provided the required input for a simplified cost model aimed at detecting the main contributions to the total cost. Representative ranges of air contactor cost (2,000 – 50,000 $/m³), heat price (0.01 – 0.1 $/kWh) and electricity price (0.01 – 0.1 $/kWh) were considered in the economic analysis [22]. ILs-based DAC systems were benchmarked to current DAC processes reported in open literature, drawing guidelines for future developments.

2. Molecular and process simulation methodology

2.1. CO₂-IL isotherms and cyclic capacity estimation

The CO₂ absorption isotherm in AHA-ILs was described by a thermodynamic model successfully applied in previous works (Eq. (1). It combines both chemical and physical chemical absorption using a chemical equilibrium constant together with Henry's Law [43,45,46]. This allows to compute the molar ratio of CO₂ absorbed per mol of IL, z:

$$z = \frac{P_{CO_2}}{K_H - P_{CO_2}} + \frac{K_{eq} \cdot P_{CO_2} \cdot C}{K_H + K_{eq} \cdot P_{CO_2}} \tag{1}$$

where P_{CO2} is the CO₂ partial pressure in bar, K_H is the CO₂ Henry's law constant in the IL in bar, K_{eq} is the reaction equilibrium constant and C is an empirical ratio representing the IL available to react with the CO₂ molecule whose value is fixed to 0.9 as reported in AHA-ILs literature [45–47].

On the one hand, the CO₂ chemical absorption was represented by a 1:1 reversible reaction (IL + CO₂ ⇌ PROD) in which CO₂ binds to a heterocyclic nitrogen of the anion to generate the reaction product (PROD) as also discussed elsewhere [45,46]. Thereby, only the anion was considered in the 1:1 reaction mechanism, since all proposed ILs are based on trihexyltetradecylphosphonium ([P₆₆₆₁₄]) cation [45]. The chemical absorption equilibrium constant (K_{eq}) was calculated at different temperatures by Van't Hoff equation (Eq. (2)) and implemented into Aspen Plus equilibrium reaction using the temperature dependence parameters of its Arrhenius relationship (Eq. (3)).

$$\ln K_{eq} = \frac{\Delta S_R}{R} - \frac{\Delta H_R}{RT} \tag{2}$$

$$\ln K_{eq} = A_1 + \frac{B_1}{T} \tag{3}$$

For this purpose, the molecular geometries of the 26 AHA-ILs and the reaction products were optimized by Turbomole 7.4 software using the B3-LYP DFT-functional paired with def2-TZVP basis set, DFT-D3 dispersion term and COSMO solvation effect to later calculate the reaction enthalpy (ΔH_R), Gibbs free energy (ΔG_R) and entropy (ΔS_R) through vibrational frequency calculations. The partition function at 298 K and a scaling factor of 0.95 were counted when estimating ΔH_R, ΔG_R and ΔS_R of the molecules. The thermochemical data for the reactions were determined as the difference between the sum of the contributions of the products and the reactants as described in aforementioned literature [45,46].

On the other hand, the CO_2 physical absorption was described by Henry's Law. K_H of CO_2 in AHA-ILs can be obtained from COSMO-RS calculations at different temperatures and included into Aspen Properties using the same Arrhenius equation (Eq. (4) and following the procedure described in detail elsewhere [43,45,46].

$$\ln K_H = A_2 + \frac{B_2}{T} \tag{4}$$

An experimental correction factor of 0.73, which was derived from comparison of COSMO-RS to experimental literature data of CO_2 K_H values in ILs, was applied to the predicted values that were later incorporated into Aspen Plus Henry's Law definition. A detailed explanation of this isotherm prediction method can be found in preceding works [45,46]. Both equilibrium and Henry's Law constants of the 26 molecular-designed ILs are collected in Table S1 of Supplementary Material. The estimated CO_2 absorption isotherms at 293 and 373 K can be found in Figure S1 of Supplementary Material. Moreover, these predicted CO_2-IL absorption isotherms allowed calculating the cyclic working capacity of the molecular-designed AHA-ILs, which is the difference between the equilibrium CO_2 loading at absorption and at desorption conditions, required to analyze which ILs match the minimum thermodynamic requirements for a viable DAC process.

2.2. Component definition and property method specification in Aspen plus

The IL-based DAC process was modelled using Aspen Plus v12. Since the molecular-designed AHA-ILs are not implemented by default in Aspen Plus databanks, they had to be introduced as pseudo-components following the successful multiscale COSMO-based/Aspen Plus methodology [48]. Based on COSMOSAC property method (in code 1 in Aspen

Properties, COSMOSAC method by Sandler et al. [49]), it requires quantum chemical structure optimizations at B-P86/TZVP level plus COSMO-RS calculations of molecular weight, boiling point, density, molecular volume and the sigma-profile for all AHA-ILs and their reaction products to fully specify the properties environment for Aspen Plus calculations [43,45]. To also describe the CO_2 mass transfer kinetics in the proposed AHA-ILs, the experimental temperature dependent viscosity (μ) data of $[P_{66614}][4\text{-}BrPyra]$ were included using Andrade's equation (Eq. (5) due to its intermediate viscosity values among reported AHA-ILs (see Figure S2 of Supplementary Material). COSMOSAC computes the physical absorption of the remaining air's components in ILs. Thermodynamic properties, chemical reaction and kinetic parameters used to define the CO_2-ILs systems in Aspen Plus simulations are summarized in Table S2 of Supplementary Material.

$$\ln \mu = M_1 + \frac{M_2}{T} \tag{5}$$

2.3. DAC process scheme

The ILs-based DAC process layout is shown in Fig. 1. Air enters the contactor via a blower, which compensates for the pressure drops. CO_2 is removed by chemical absorption with the IL in the air contactor unit designed by Carbon Engineering, which adapted commercial cooling towers to fit liquid scrubbing for DAC application [12,13]. The adopted technology was formerly applied and studied in alkali and amine scrubbing processes and it offered an evident improvement over conventional absorption columns at DAC conditions [16,21,22]. The CO_2-rich solvent stream is then preheated in a conventional heat exchanger using the hot CO_2-lean solvent stream (regenerated IL), before entering the flash column in which the regeneration of the IL and the desorption of CO_2 take place. CO_2 is dehydrated in a condenser and compressed for transport and storage, and the regenerated IL is recirculated to the air contactor after conditioning pressure and temperature.

2.4. DAC process simulation

Advanced rate-based simulations in Aspen Plus were carry out to address the process analysis for IL-based DAC technology. In all cases, the DAC process treats air at exemplary ambient conditions (relative humidity of 43% and a CO_2 content of 400 ppm [22]). Table 1 reports the inlet air stream conditions and compositions. The air blower is modeled with an isentropic compressor model and calculates the energy required to introduce the air into the air contactor.

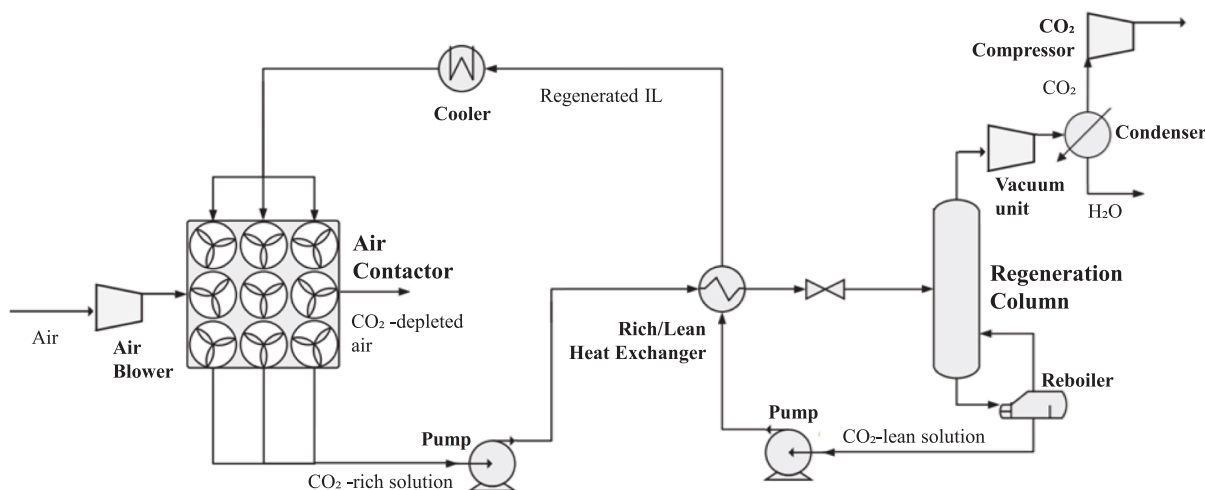The air contactor for CO_2 absorption was modeled using Aspen Plus's

Fig. 1. ILs-based DAC process diagram.

Table 1
Air stream properties.

Temperature (K)		293
Pressure (bar)		1.0
Composition (%mol)	x_{CO_2}	0.04
	x_{N_2}	77.95
	x_{O_2}	21.00
	x_{H_2O}	1.01

RadFrac column model. Rate-based calculations were performed to consider mass transfer limits in the process, and Aspen Plus's equilibrium reaction was employed to describe the chemical reaction between CO_2 and each IL, whose K_{eq} equation must be specified with the temperature dependence parameters (see Table S2 of Supplementary Material) as explained before [43,45]. The reaction occurs in the liquid phase and the equilibrium constant basis is mole-fraction based. To reproduce the cross-flow configuration of Carbon Engineering's design, the air contactor was simulated using three rate-based RadFrac blocks arranged in parallel with vapor plug flow as reported in previous work [22]. The height and diameter of each block were fixed to reproduce the inlet area and packing depth of Carbon Engineering's air contactor [22]. Regarding the IL regeneration, a rigorous continuous stirred tank reactor block with the same equilibrium reaction as the air contactor was adopted to model the flash desorption stage, since solvent regeneration is typically accomplished at operating conditions close to equilibrium. We use a single stage separation because its proven efficiency and simplicity [50] facilitates the calculation of the large sensitivity carried out. The condenser that dehydrates CO_2 was modeled by a flash separator block.

A technical analysis was carried out by evaluating several operating and design variables to determine the optimal performance of the different DAC systems, where optimality is defined by the exergy consumption for the separation and the productivity of the process (see below for definitions). The analysis included testing temperatures from 293 to 323 K and a mass flow range of 5 – 50 t/h for the IL entering the air contactor, different air velocities (1 – 3 m/s) in the air contactor, and multiple regeneration temperatures and pressures ranges of 373 – 393 K and 0.1 – 1 bar, respectively. This resulted in a sensitivity analysis of 3,524 cases. The energy consumed when desorbing at vacuum pressure was estimated by a compressor block simulated via isentropic transformation adjusted with efficiency; this emulates the pressure change from the corresponding vacuum pressure to ambient conditions (1 bar). The pump model estimates the power needed to circulate the solvent stream between the air contactor and the regeneration unit. Compression and pumping efficiencies were fixed from state-of-the-art values [42,51]. The energy demand for the following CO_2 compression to supercritical conditions was also included, and it was fixed to be 0.28 MJ/kg_{CO_2} following previous DAC publication [22]. Table 2 summarizes the main specifications adopted as dimensions, packing type, operating conditions, and design variables. The mass-specific exergy (Eq. (6) and productivity (Eq. (7) were used to drive the process optimization. Given the different types of energy input to the process, i.e. heat and electricity, we used exergy - as indicator of operating costs - to compare the different process conditions. More specifically, by computing mass-specific exergy (Eq. (6) we aim to identify the process conditions that require the minimum useful energy as input to separate one kg of CO_2, allowing for a fair balance between electricity (pure exergy) and heat at low temperature (low exergy). This mass-specific exergy is not to be confused with the specific exergy content of the produced CO_2 stream. In contrast, productivity (Eq. (7) is considered a proxy of the equipment size and cost.

$$e_{CO_2} = \frac{1}{\dot{m}_{CO_2}} \cdot \left[\dot{Q}_{reb} \cdot \left(1 - \frac{T_0}{T_{reb}} \right) + \dot{W}_{blower} + \dot{W}_{vac} + \dot{W}_{comp} + \dot{W}_{pump} \right] \quad (6)$$

Table 2
Main specifications and design variables of DAC processes simulations.

Equipment	Variable	Units	Value
Air contactor	Number of blocks	–	3
	Number of stages per block	–	30
	Diameter	m	5.64
	Height	m	2.32
	Packing type	–	Sulzer 250Y
	Pressure	bar	1
	IL mass flow	t/h	5–50
Regeneration column	Pressure	bar	0.1–1
	Reboiler temperature	K	373–393
Condenser	Pressure	bar	1
	Temperature	K	303
Cooler	Pressure drop	bar	0
	Outlet temperature	K	293–323
Rich/Lean Heat exchanger	Hot/cold outlet temperature approach	K	10
Air blower	Isentropic efficiency	%	56
	Mechanical efficiency	%	98
	Air velocity	m/s	1–3
Vacuum unit	Isentropic efficiency	%	60
	Mechanical efficiency	%	95
	Discharge pressure	bar	1
Pump	Power efficiency	%	70
	Driver efficiency	%	95

$$Pr = \frac{\dot{m}_{CO_2}}{V_{contactor}} \quad (7)$$

where e_{CO_2} is the mass-specific exergy to separate CO_2 from air, $\dot{m}_{CO_2}$ is the mass rate of captured CO_2, $\dot{Q}_{reb}$ is the reboiler duty, T_{reb} is the reboiler temperature, T_0 is 298 K, $\dot{W}_{blower}$, $\dot{W}_{vac}$, $\dot{W}_{comp}$ and $\dot{W}_{pump}$ are the power requirement of the air blower, vacuum operation, CO_2 compressor and the pump, respectively. Pr is the productivity and $V_{contactor}$ is the volume of the air contactor.

2.5. Simplified economic evaluation

A simple economic evaluation of the DAC processes based on ILs was carried out to identify the major contributors to the total cost of these DAC plants, and to compare their cost potential with current technologies. We would like to stress that this is not a detailed economic analysis with bottom-up costing of the different components, which would be very uncertain, but it is rather a simple evaluation of the costs starting from the key cost components. The value of this analysis is therefore in the identification of the costs range, and more importantly on the trends between costs and the key design/operation parameters (the reader should refrain from identifying DAC-IL costs with one of the cost points provided in this analysis). Accordingly, we computed the total cost of CO_2 captured by simply considering the cost of utilities (electricity and steam for heating) and the air contactor cost (γ), which are proxies for operating (OPEX) and capital (CAPEX) costs, respectively. Thus, using the energy and productivity computations of the technical analysis the specific cost of CO_2 captured was estimated as a function of the electricity, steam, and air contactor prices by the following equation (Eq. (8)) [22]:

$$C_{CO_2} = \frac{\gamma}{Pr \cdot a} + c_{th} \cdot e_{th} + c_{el} \cdot e_{el} \qquad (8)$$

where Pr, e_{th} and e_{el} are the productivity, the thermal energy and the electric demand taken from the technical analysis, respectively, and a is a 20-year lifetime of the plant (operating 8,000 h/year). A range from 2,000 \$/m^3 (contactor cost calculated from [14]) to 50,000 \$/m^3 (from Hinwil Climeworks plant [4,29]) was chosen for the air contactor cost (γ) as in preceding studies [22], whereas for electricity (c_{el}) and steam (c_{th}) a realistic range of 0.01 – 0.1 \$/kWh was considered. Note that steam costs should be however lower than electricity costs when selecting a specific parameters combination.

3. Results

3.1. Selection of suitable ionic liquids

As first step for the identification of promising ILs, the cyclic working capacity of the 26 different molecular-designed AHA-ILs was predicted by DFT/COSMO-RS computations [45,46]. Calculation details of the cyclic capacity are available in Supplementary Material. Fig. 2a shows the AHA-ILs cyclic capacity estimated with ambient temperature and 400 ppm of CO_2 for the absorption step (see Table 1), a desorption temperature of 373 K and different desorption partial pressures of CO_2 (0.01 – 0.4 bar).

Fig. 2a shows that there are 9 ILs with positive cyclic capacity ranging between 0 mol/kg and 1 mol/kg (1.02 mol/kg for [P$_{66614}$][5-CH$_3$Im] and 1.04 mol/kg for [P$_{66614}$][Im]). This is achieved below atmospheric conditions. In fact, for partial pressures above 0.16 bar the cyclic capacity value of the 9 positive ILs turn negative, which suggests vacuum operation for an efficient desorption or solvent regeneration to maximize its cyclic working capacity [52]. In contrast, the remaining 17 of the 26 ILs considered in this work exhibited an inadequate cyclic capacity (equal or lower than 0 mol/kg) for DAC purposes. Fig. 2b shows the dependence of the cyclic capacity with the enthalpy of the reaction between CO_2 and the AHA-IL. An optimum for the cyclic capacity can be observed around −55 – −60 kJ/mol for three different desorption partial pressures, as heat of reaction can be tuned to enhance the cyclic capacity as demonstrated in previous works [40,45]. This optimum corresponds to [P$_{66614}$][3-BrPyra] (-55.9 kJ/mol), [P$_{66614}$][5-CH$_3$Im] (-57.8 kJ/mol) and [P$_{66614}$][Im] (-59.8 kJ/mol) absorbents. Although AHA-ILs below the optimal reaction enthalpy range (-55 – −60 kJ/mol) are easier to regenerate, their CO_2 capacity is likely too small for DAC applications. Fig. 2b also shows that severe vacuum in desorption stage increases the cyclic capacity but maintains the optimal range of CO_2-IL reaction enthalpy.

A possible range of desorption temperatures (320 – 400 K) was tested alongside the desorption pressure. Fig. 3a shows the ILs cyclic capacity calculated with a desorption pressure of 0.1 bar and different desorption temperatures. As expected, the same 9 ILs exhibited good cyclic capacity values for DAC with respect to the desorption temperature as shown in Fig. 3a. Increasing the desorption temperature improves the cyclic capacity up to 0.8 mol/kg at 400 K for the best cases as [P$_{66614}$][5-CH$_3$Im] (0.82 mol/kg) and [P$_{66614}$][Im] (0.78 mol/kg), since it favors the regeneration of the AHA-IL [52]. A minimum regeneration temperature of 373 K is required to obtain positive cyclic capacities at DAC conditions. [P$_{66614}$][3-BrPyra] (-55.9 kJ/mol), [P$_{66614}$][5-CH$_3$Im] (-57.8 kJ/mol) and [P$_{66614}$][Im] (-59.8 kJ/mol) achieved again the best cyclic capacity values at different desorption temperatures. Accordingly, from a thermodynamic perspective, [P$_{66614}$][3-BrPyra], [P$_{66614}$][5-CH$_3$Im] and [P$_{66614}$][Im] were identified as the three most promising AHA-ILs for DAC.

3.2. Techno-economic analysis of IL-based DAC processes

The three most promising AHA-ILs identified in the molecular screening step ([P$_{66614}$][3-BrPyra], [P$_{66614}$][5-CH$_3$Im] and [P$_{66614}$][Im]) were evaluated for DAC in terms of productivity and mass-specific exergy by means of process simulation. Fig. 4 shows the results for [P$_{66614}$][Im] in terms of productivity and mass-specific exergy, depending on the air velocity and IL mas flow. Common trends can be found for all ILs (see Figure S2 of Supplementary Material). For each air velocity value, increasing the productivity leads to an exergy reduction up to an optimal operation range from which exergy increments exponentially with higher productivity. Higher air velocity leads to greater productivity, but it also increments the exergy demand because the power consumption of the blower is increased. Concurrently, the IL mass flow required to achieve higher productivity is also higher, since there is more CO_2 to be captured, which contributes to higher mass-specific exergy consumption by rising solvent heating/cooling duties and pumping needs. On the other hand, a minimum in the exergy demand was found in the 2 – 20 t/h range for each air velocity value. Further increments in the IL mass flows only drive to higher exergy requirement, since productivity is independent of the mass flow above ≈ 20 t/h. In this sense, [P$_{66614}$][Im] exhibits lower exergy values than [P$_{66614}$][3-BrPyra] and [P$_{66614}$][5-CH$_3$Im] due to the lower quantity of IL required. The minimum exergy consumption is achieved at: 28.6 kg$_{IL}$/kg$_{CO2}$ for [P$_{66614}$][Im], 50.4 kg$_{IL}$/kg$_{CO2}$ for [P$_{66614}$][5-CH$_3$Im] in Figure S2, and 62.9 kg$_{IL}$/kg$_{CO2}$ for [P$_{66614}$][3-BrPyra] in Figure S2 at 1.4 m/s.

Subsequently, the effect of the temperature of the solvent stream entering the air contactor was analyzed. Fig. 5 illustrates productivity and exergy with respect to the IL inlet temperature and to IL mas flow for
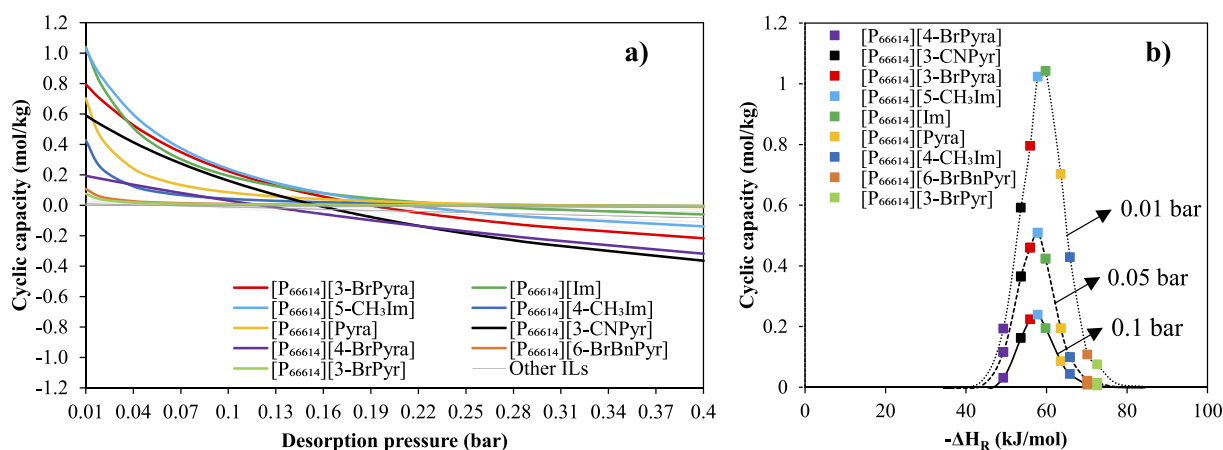

Fig. 2. AHA-ILs cyclic capacity with respect to (a) the desorption partial pressure of CO_2 and (b) the enthalpy of reaction. 293 K, 1 bar and 400 ppm of CO_2 were assumed to calculate the absorption capacity, whereas the desorption capacity was estimated at 373 K and varying the pressure. Colored ILs are suitable for DAC.
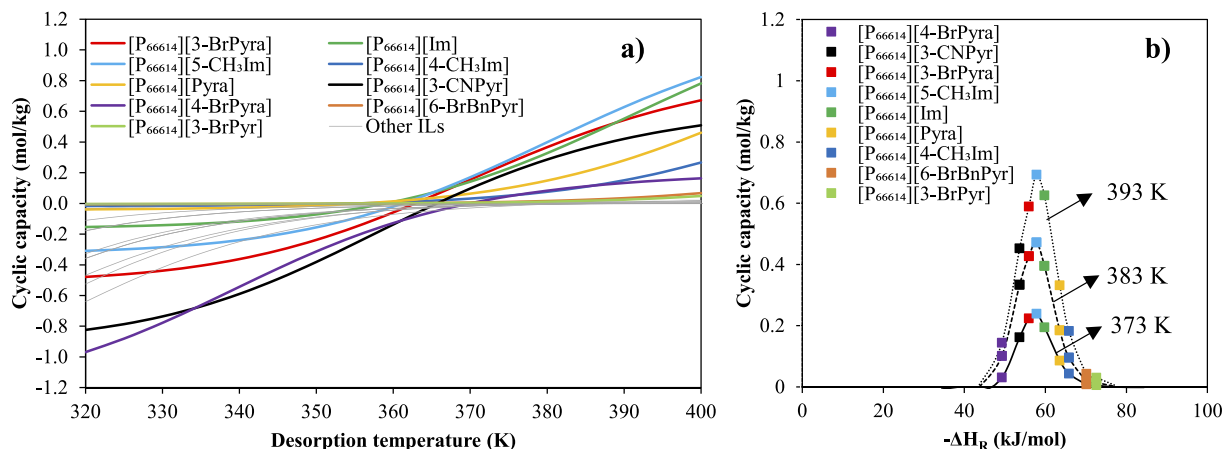
Fig. 3. AHA-ILs cyclic capacity with respect to (a) the desorption temperature and (b) the enthalpy of reaction. 293 K, 1 bar and 400 ppm of CO_2 were considered to calculate the absorption capacity, whereas the desorption capacity was estimated at 0.1 bar and varying temperature. Colored ILs are suitable for DAC.
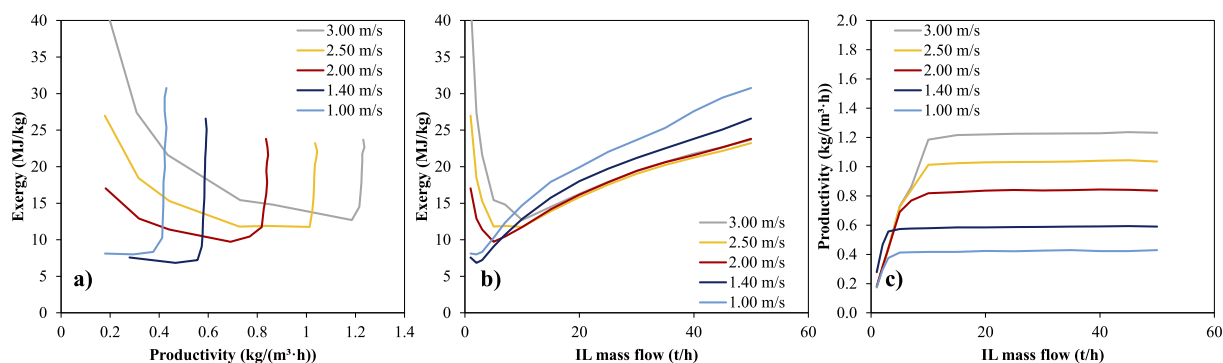

Fig. 4. Exergy vs. productivity (a), exergy vs. IL mass flow (b), and productivity vs. IL mass flow (c) planes of DAC process based on $[P_{66614}][Im]$ depending on the air velocity. Results calculated for an IL inlet temperature of 293 K, an absorption operated at and 1 bar, and desorption working at 373 K and 0.1 bar.
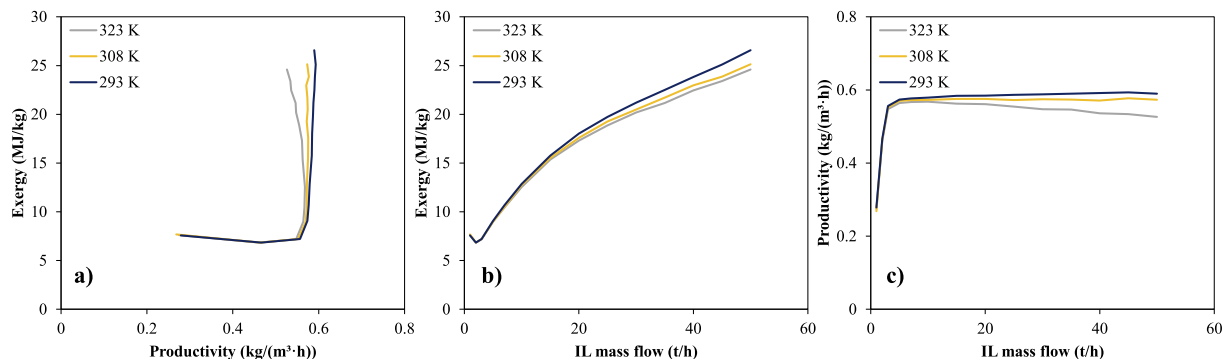

Fig. 5. Exergy vs. productivity (a), exergy vs. IL mass flow (b), and productivity vs. IL mass flow (c) planes of DAC process based on $[P_{66614}][Im]$ depending on the IL temperature. Results calculated for an air velocity of 1.4 m/s, an absorption operated 1 bar, and desorption working at 373 K and 0.1 bar.

$[P_{66614}][Im]$. A negligible effect of the IL inlet temperature can be noticed for the three ILs tested, because the higher air flow rate (1.4 m/s is equivalent to 151.1 t/h approx.) at ambient temperature (293 K) controls the temperature of the absorption. At high productivity and great IL mass flow (above 30 t/h), an exergy decrease with temperature is observed. Minimum exergies can be seen in the 1 – 5 t/h range at these conditions. Regarding the IL (see Figure S3), a minimum exergy of 6.8 MJ/kg_{CO2} is seen for $[P_{66614}][Im]$, whereas $[P_{66614}][5\text{-}CH_3Im]$ and $[P_{66614}][3\text{-}BrPyra]$ increment the exergy to 9.0 MJ/kg_{CO2} and 9.8 MJ/kg_{CO2}, respectively, at both 293 and 308 K.

Moving to the regeneration step, Fig. 6 shows the effect of different regeneration temperature and IL mas flow on productivity and exergy

for $[P_{66614}][Im]$. Increasing the reboiler temperature slightly improves the productivity at the expense of higher exergy demand for $[P_{66614}][Im]$ but also for the rest of ILs. Concerning the different ILs (see Figure S4 of Supplementary Material), the desorption temperature effect amplifies when reducing the enthalpy of reaction; $[P_{66614}][Im]$ presents lower exergy demands than $[P_{66614}][5\text{-}CH_3Im]$ and $[P_{66614}][3\text{-}BrPyra]$ (below 10 MJ/kg_{CO2} for all temperatures, see Figure S4) because its favored chemical absorption leads to higher CO_2 capture rates with less quantity of solvent involved (26.8 kg_{IL}/kg_{CO2} for $[P_{66614}][Im]$, 44.9 kg_{IL}/kg_{CO2} for $[P_{66614}][5\text{-}CH_3Im]$ in Figure S4, and 73.5 kg_{IL}/kg_{CO2} for $[P_{66614}][3\text{-}BrPyra]$ in Figure S4 at 393 K).

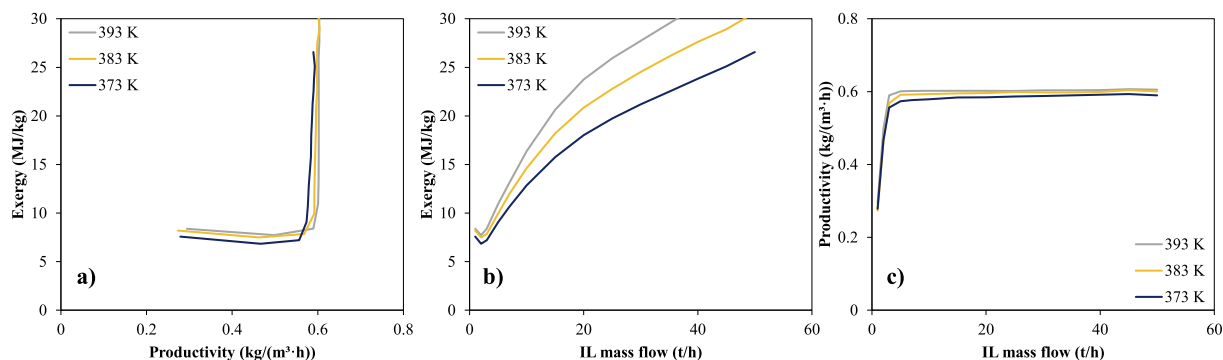Finally, the effect of vacuum pressure and the IL mass flow on

Fig. 6. Exergy vs. productivity (a), exergy vs. IL mass flow (b), and productivity vs. IL mass flow (c) planes of DAC process based on [P$_{66614}$][Im] depending on the desorption temperature. Results calculated for an air velocity of 1.4 m/s, an absorption operated at 293 K and 1 bar, and desorption working at 0.1 bar.

productivity and exergy when using [P$_{66614}$][Im] is shown in Fig. 7. It can be noted that higher pressure decreases the exergy demand (from 7.7 to 5.4 MJ/kg$_{CO2}$ for [P$_{66614}$][Im], from 10.2 to 6.6 MJ/kg$_{CO2}$ for [P$_{66614}$][5-CH$_3$Im] in Figure S5, and from 12.2 to 7.1 MJ/kg$_{CO2}$ for [P$_{66614}$][3-BrPyra] in Figure S5, comparing 0.1 to 1 bar), but it also reduces the productivity (from 0.50 to 0.39 kg/(m^3·h) for [P$_{66614}$][Im], from 0.45 to 0.39 kg/(m^3·h) for [P$_{66614}$][5-CH$_3$Im] in Figure S5), and from 0.45 to 0.32 kg/(m^3·h) for [P$_{66614}$][3-BrPyra] in Figure S5, comparing 0.1 to 1 bar), since the IL is regenerated to a lesser extent and therefore captures less CO$_2$. It follows that the required mass flow of IL is smaller when operating at low pressure (26.8 vs. 51.8 kg$_{IL}$/kg$_{CO2}$ for [P$_{66614}$][Im], 44.9 vs. 84.8 kg$_{IL}$/kg$_{CO2}$ for [P$_{66614}$][5-CH$_3$Im] in Figure S5, and 73.5 vs. 103.6 kg$_{IL}$/kg$_{CO2}$ for [P$_{66614}$][3-BrPyra] in Figure S5, comparing 0.1 to 1 bar), drastically reducing the reboiler duty and consequently the exergy demand. Suitable pressure values are between 0.75 and 0.5 bar because at high productivity the mass-specific exergy is still low. [P$_{66614}$][Im] exhibited the best productivity and mass-specific results anew, in comparison with [P$_{66614}$][5-CH$_3$Im] and [P$_{66614}$][3-BrPyra] (see Figure S5 of Supplementary Material).

Bringing together the results shown in the previous figures per each design parameter (i.e. air velocity, IL mass flow, inlet and regeneration temperature, vacuum pressure), the overall Pareto frontier for exergy, energy and productivity was extracted from all simulated cases and represented in Fig. 8a, 9a and 10a. The region above the curve is suboptimal, whereas that below is unfeasible. Table S3 of Supplementary Material summarizes the operating conditions of the extremes of the Pareto (Points A and B). Both productivity and exergy requirement change significantly along the Pareto of the three AHA-ILs, highlighting the relevance of selecting proper design and operating conditions. The productivity achieved on the minimum-exergy (Point A, ≈ 0.5 kg/(m^3·h)) and maximum-productivity (Point B, ≈ 1.3 kg/(m^3·h)) cases is analogous for the three AHA-ILs as illustrated in Fig. 8a, 9a and 10a, and summarized in Table 3. This is because the captured CO$_2$ on each point is

similar: Point A: 68.2, 71.4 & 76.9 kg/h; and Point B: 190.6, 192.0 & 192.4 kg/h for [P$_{66614}$][3-BrPyra], [P$_{66614}$][5-CH$_3$Im] and [P$_{66614}$][Im], respectively. On the contrary, the exergy (energy) results reported in Figs. 8, 9 and 10, and Table 3 for these operational points differ a lot between AHA-ILs (Point A: 5.44 (15.15) MJ/kg for [P$_{66614}$][Im], 6.15 (19.46) MJ/kg for [P$_{66614}$][5-CH$_3$Im], 7.14 (23.09) MJ/kg for [P$_{66614}$][3-BrPyra] and Point B: 16.73 (35.42) MJ/kg, 21.34 (48.31) MJ/kg, 26.43 (63.56) MJ/kg, for [P$_{66614}$][Im], [P$_{66614}$][5-CH$_3$Im] and [P$_{66614}$][3-BrPyra], respectively). The energy demand breakdown for points A and B of the Pareto curves is represented in Fig. 8b, 9b and 10b. It can be noted that, for both extremes of the Pareto, the reboiler duty is the main part of the energy requirement for all AHA-ILs. Thus, the total energy required differs from one AHA-IL to another because the reboiler duty depends on the mass flow, which is determined not only by the AHA-IL cyclic capacity but also by its molar mass (Table S1). [P$_{66614}$][Im] reduces the heating demand up to 13.3 MJ/kg in Point A and 24.6 MJ/kg in Point B, and hence attains the most energy-efficient DAC system based on ILs. This is a result of the most favored chemical capture and lowest molar mass and therefore lowest mass flow (Point A: 7 t/h of [P$_{66614}$][3-BrPyra], 5 t/h of [P$_{66614}$][5-CH$_3$Im] and 3 t/h of [P$_{66614}$][Im]). Changing the [P$_{66614}$] cation for another with lower molecular weight as triethyl(octyl)phosphonium ([P$_{2228}$]) could further reduce the mass flow of solvent [43,47]. Moreover, the reboiler duty increases dramatically when moving toward higher productivity as higher IL mass flows are involved (Point B: 45 t/h of [P$_{66614}$][3-BrPyra], 25 t/h of [P$_{66614}$][5-CH$_3$Im] and 15 t/h of [P$_{66614}$][Im]). A similar trend can be observed for secondary energy contributors, as the air blower and vacuum operation, which require more energy at higher productivity. On the other hand, the energy required by the air blower for both operational points (A and B) is very similar for all AHA-ILs because they are operating with equal air velocities (1.4 m/s for Point A and 3 m/s for Point B), whereas vacuum demand decreases significantly on Point B when changing the AHA-IL, because the lower mass flow of [P$_{66614}$][Im] is less saturated in
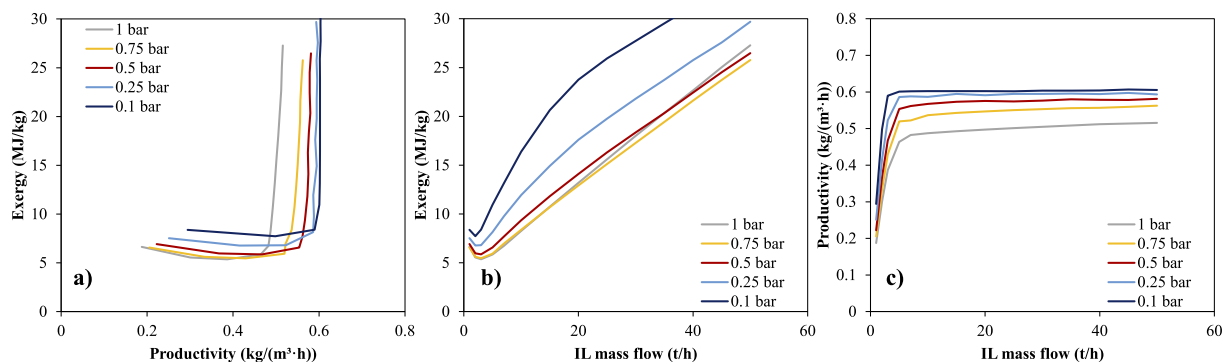

Fig. 7. Exergy vs. productivity (a), exergy vs. IL mass flow (b), and productivity vs. IL mass flow (c) planes of DAC process based on [P$_{66614}$][Im] depending on the desorption pressure. Results calculated for an air velocity of 1.4 m/s, an absorption operated at 293 K and 1 bar, and desorption working at 393 K.
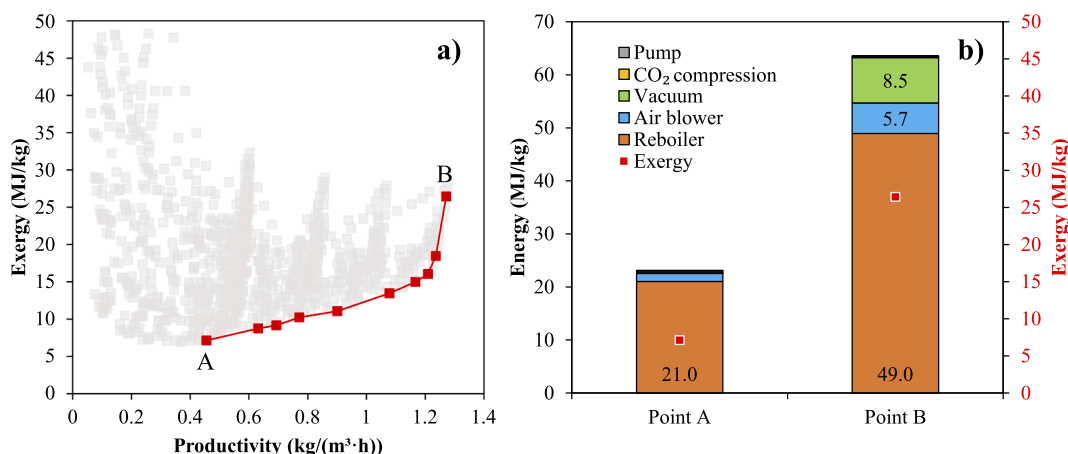
Fig. 8. (a) Exergy vs. productivity Pareto front for $[P_{66614}][3\text{-BrPyra}]$-based DAC process, together with (b) the breakdown of the energy demand for the two extremes; point A: minimum exergy consumption and point B: maximum productivity.

Table 3
Exergy and energy consumption, as well as productivity of reference DAC technologies and the IL-based processes for the two extreme Pareto points A and B, referring to the Pareto charts shown in Figs. 9, 10 and 11.

	Exergy (MJ/kg)		Energy (MJ/kg)		Productivity (kg/(m³·h))	
	A	B	A	B	A	B
$[P_{66614}][3\text{-Pyra}]$	7.14	26.43	23.09	63.56	0.46	1.27
$[P_{66614}][5\text{-CH}_3\text{Im}]$	6.15	21.34	19.46	48.31	0.48	1.28
$[P_{66614}][\text{Im}]$	5.44	16.73	15.51	35.42	0.51	1.28
Alkali-scrubbing [22]	6.21	6.48	6.21	6.48	0.18	0.45
Amine-scrubbing [22]	5.59	13.13	20.04	49.32	0.75	1.08
Solid sorbent[a] [22]	1.81	2.1	7.96	8.68	3.8	10.6

[a] Solid sorbent process calculated with an exemplary sorbent isotherm.

water and this reduces the vapor flow to be removed in the regeneration unit (all ILs operate at 0.1 bar of vacuum pressure on this point). In brief, it can be concluded that $[P_{66614}][\text{Im}]$ achieves a less energy-demanding DAC system than $[P_{66614}][5\text{-CH}_3\text{Im}]$ and $[P_{66614}][3\text{-BrPyra}]$ for similar

productivity due to its enhanced cyclic capacity (Cyclic capacity on Point A and Point B are: 0.2 and 0.1, 0.3 and 0.2 and 0.6 and 0.3 mol/kg for $[P_{66614}][3\text{-BrPyra}]$, $[P_{66614}][5\text{-CH}_3\text{Im}]$ and $[P_{66614}][\text{Im}]$, respectively). Capture rates on Point A and Point B are: 73.8 and 96.2, 77.2 and 96.9, and 83.2 and 97.1 % for $[P_{66614}][3\text{-BrPyra}]$, $[P_{66614}][5\text{-CH}_3\text{Im}]$ and $[P_{66614}][\text{Im}]$, respectively. High CO_2 purities exceeding 95 %mol are achieved in all cases and water with a purity higher than 99 %mol could be co-produced, which would be particularly interesting in water-distressed areas. The resulting values for CO_2 and water purities in the corresponding product streams (see Fig. 1), CO_2 concentration in the CO_2-depleted air stream and CO_2 recovery are summarized in Table S4 of Supplementary Material for Pareto points A and B of each IL.

Table 3 also reports the productivity and mass-specific exergy and energy values of different DAC technologies studied using the same air contactor design [22]. In terms of exergy demand, all ILs-based DAC systems are comparable or slightly lower (5.44 MJ/kg of $[P_{66614}][\text{Im}]$ vs. 6.21 MJ/kg) than the reference alkali-scrubbing process while attaining similar productivity (0.45 – 0.51 kg/(m³·h)). However, they require higher energy (15.51 MJ/kg of $[P_{66614}][\text{Im}]$ vs. 6.48 MJ/kg) than their alkali counterpart. According to Table 3 data, the most

Fig. 9. (a) Exergy vs. productivity Pareto front for $[P_{66614}][5\text{-CH}_3\text{Im}]$-based DAC process, together with (b) the breakdown of the energy demand for the two extremes; point A: minimum exergy consumption and point B: maximum productivity.
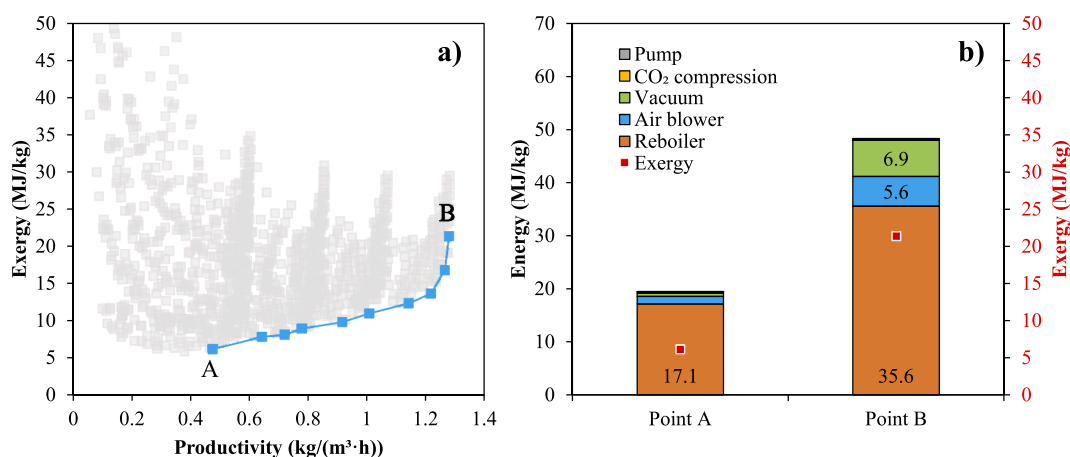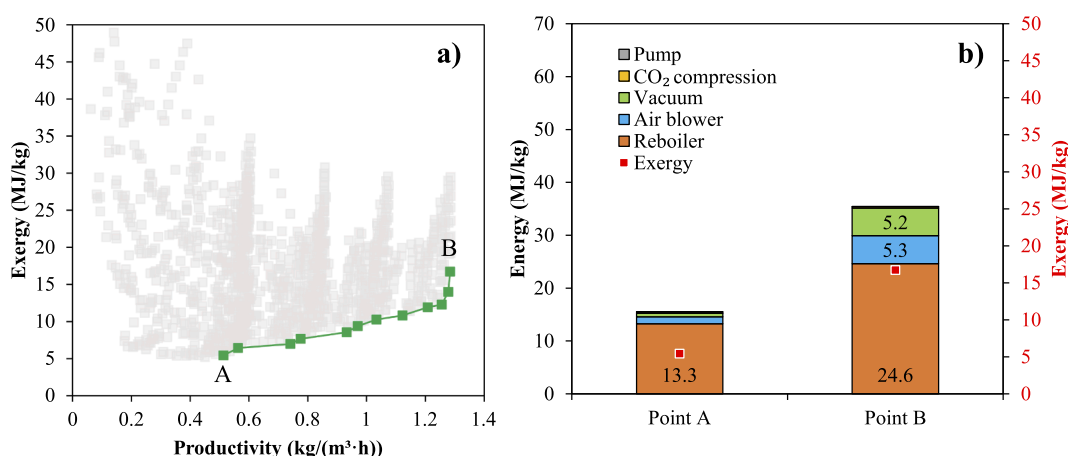
Fig. 10. (a) Exergy vs. productivity Pareto front for $[P_{66614}][Im]$-based DAC process, together with (b) the breakdown of the energy demand for the two extremes; point A: minimum exergy consumption and point B: maximum productivity.

suitable IL, $[P_{66614}][Im]$, exhibits a less-intensive exergy (energy) process than amine-scrubbing 5.44 (15.51) MJ/kg vs. 5.59 (20.04) MJ/kg at the expense of reducing the productivity from 0.75 to 0.51 kg/(m³·h). In contrast, for top productivity (Point B), $[P_{66614}][Im]$ consumes more exergy than the MEA-based system (16.73 vs.13.13 MJ/kg) because of the vacuum operation and air velocity required, but less energy (35.42 vs. 49.32 MJ/kg) due to a lower reboiler duty (24.6 vs. 48.16 MJ/kg) [22]. It is worth however stressing that these energy values would not be realistic for commercial operation and that the maximum productivity points would not be pursued in a real plant. The steep Pareto front of IL-based DAC technologies indicates in fact that one optimal operating point is eventually present, and productivity could only be slightly increased at great energy expenditures.

The results of the simplified economic assessment are shown in Figs. 11 and 12. Fig. 11 reports the maps of the costs of the IL-based DAC systems as function of the heat and electricity prices (0.01 – 0.1 $/kWh), and the air contactor cost (2,000 – 50,000 $/m³). The total cost was calculated using Point A (lowest exergy and energy consumption) from the Pareto front of each IL (Figs. 8, 9 and 10). Although the full heat-electricity price plane is represented for completeness, cases where electricity is cheaper than heat should be disregarded (only possible under very specific boundary conditions).

It can first be noted that the low productivity achieved on the minimum-exergy/energy operation case for all ILs (Point A in the Pareto chart) makes the total cost strongly dependent on the plant cost. Consequently, the DAC-IL costs are strongly function of the contactor cost. However, because of the large variation in the energy requirements along the Pareto front, the total plant cost varies significantly with the heat price (the reboiler duty is dominating the energy demand). For example, in the low contactor cost area (2,000 $/m³) the plant cost would still span from below 200 $/$t_{CO2}$ to above 600 $/$t_{CO2}$ (92 – 669 $/$t_{CO2}$ for $[P_{66614}][3\text{-BrPyra}]$, 80 – 567 $/$t_{CO2}$ for $[P_{66614}][5\text{-CH}_3\text{Im}]$ and 67 – 455 $/$t_{CO2}$ for $[P_{66614}][Im]$). Moreover, it is worth stressing that this contactor cost may be very difficult to achieve even in the case of high learning rates. While the strong dependency on heat price is clearly observed for all AHA-ILs, it is especially noticeable when higher quantity of IL is involved, as in Fig. 11a for $[P_{66614}][3\text{-BrPyra}]$. Not surprisingly, DAC-IL processes are not significantly affected by the electricity price (this would indeed not be true if heat were to be supplied via a heat pump). If the results are used to plot the productivity-

total cost function, as represented in Fig. 12, it can be observed for any of the three AHA-ILs that the minimum cost does not correspond to the minimum exergy point (Point A), unless the contactor cost is (close to) 2,000 $/m³ (Fig. 12a). The cost penalty of vacuum operation at high price of electricity is instead behind the cost fluctuations shown in the Pareto curve of each AHA-IL.

Regarding the solvents, $[P_{66614}][Im]$ exhibits more favorable behavior of the costs compared to $[P_{66614}][3\text{-BrPyra}]$ and $[P_{66614}][5\text{-}CH_3\text{Im}]$. This is due to the significantly smaller mass flow, and hence energy requirement. If we compare the cost of $[P_{66614}][Im]$ with previous cost estimates for alkali and amine scrubbing, we find that DAC-IL ($[P_{66614}][Im]$) is in line with the other technologies: when using a plant cost of 25,000 $/m³, a heat price of 0.05 $/kWh and an electricity price of 0.1 $/kWh, DAC-IL requires 506 $/$t_{CO2}$ while alkali and amine scrubbing require 419 and 537 $/$t_{CO2}$, respectively [22]. If a plant cost of 50,000 $/m³ (range of sorbent-based demonstration projects) is assumed, then $[P_{66614}][Im]$ achieves a cost of 680 $/$t_{CO2}$, close to 600 $/$t_{CO2}$, which is line with previous estimated for both solid and liquid sorbents [5,11,21,53]. In brief, these results suggest DAC-IL might be an equally good candidate for DAC applications from a cost perspective.

To conclude the process analysis, we better investigated the effect of the IL viscosity, which is a major source of uncertainty for $[P_{66614}][Im]$, and which was identified as the most promising AHA-IL for DAC application. Accordingly, a more conservative scenario was computed by increasing $[P_{66614}][Im]$ viscosity. The experimental viscosity data from $[P_{2228}][4\text{-BrIm}]$ [54], a more viscous IL than the reference $[P_{66614}]$ $[4\text{-BrPyra}]$ and with an anion based on the same heterocyclic ring ($[Im]$), was used to estimate it (see Figure S6 of Supplementary Material). Fig. 13 compares productivity and mass-specific exergy at the operational point corresponding to minimum exergy (Point A in Figs. 8, 9 and 10) using the different viscosity data. Increasing the IL viscosity reduces 14% the productivity value from 0.51 to 0.44 kg/(m³·h), in contrast to a 13% incremented mass-specific exergy from 5.44 to 6.13 MJ/kg_{CO2}. As consequence, the total cost of the DAC-IL technology increases by around 13%; from 271 $/$t_{CO2}$ to 306 $/$t_{CO2}$ assuming a plant cost of 2,000 $/m³, a heat price of 0.05 $/kWh and an electricity price of 0.1 $/kWh [22]. As expected, the IL transport properties play a significant role on the performance and economics of the DAC-IL process, which is in line with what was found for conventional carbon capture [55].
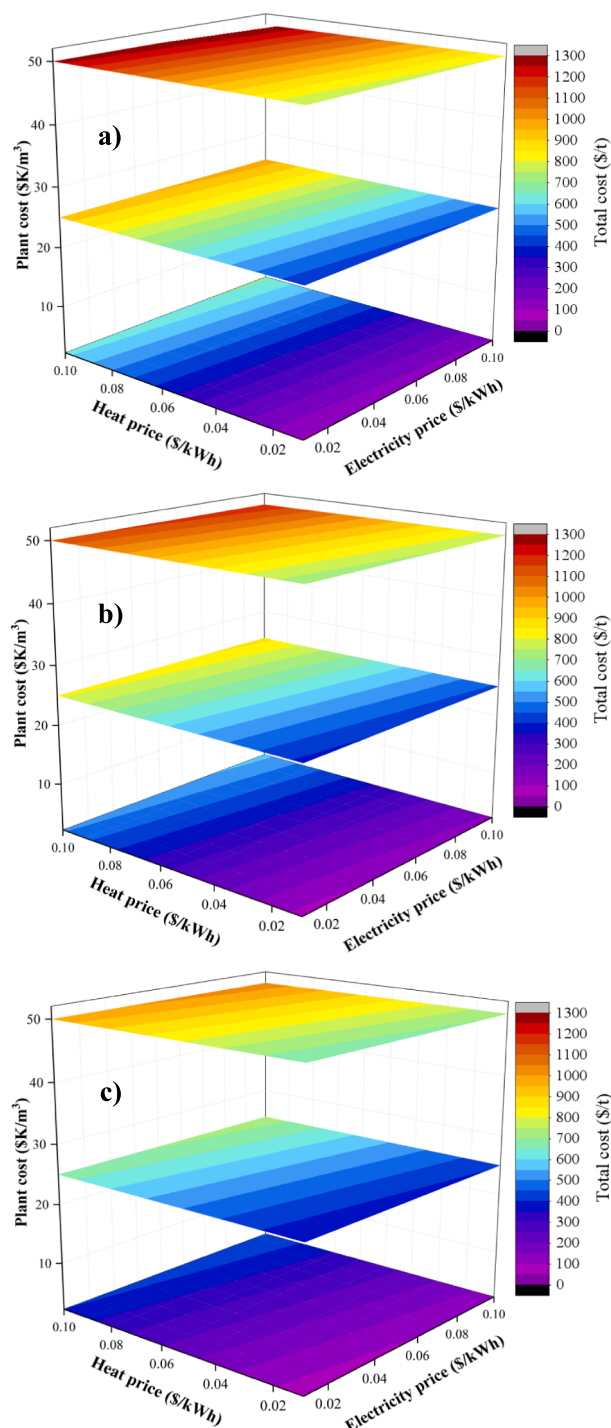
Fig. 11. Maps of the DAC-IL system cost as a function of electricity price, heat price, and plant cost for (a) $[P_{66614}][3\text{-BrPyra}]$, (b) $[P_{66614}][5\text{-CH}_3\text{Im}]$ and (c) $[P_{66614}][\text{Im}]$. Operating conditions of the minimum-exergy/energy case (Point A in the Pareto chart) were used.

Fig. 12. Cost vs. productivity Pareto front for the three different IL-based DAC processes. Cost calculated using a plant cost of 2,000 $/m^3$ (a), 25,000 $/m^3$ (b) and 50,000 $/m^3$ (c), a heat price of 0.05 $/kWh and an electricity price of 0.1 $/kWh.

4. Discussion and recommendations for improving the IL performance in DAC applications

This work has tackled for the first time the design – from molecular to process level – of a DAC application using ionic liquids. While we tried to apply a comprehensive and detailed methodology in all steps, we can certainly identify further actions for improvement. First and foremost, the selection of ILs for DAC processes should include both absorption
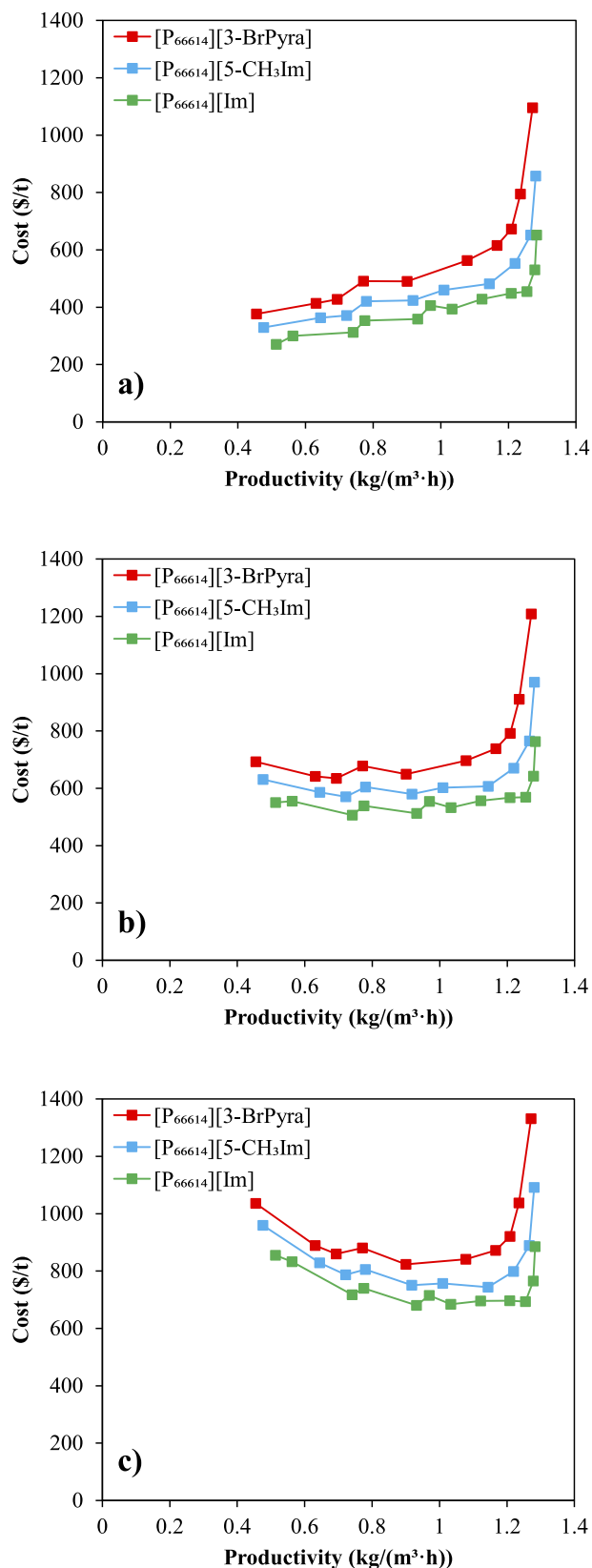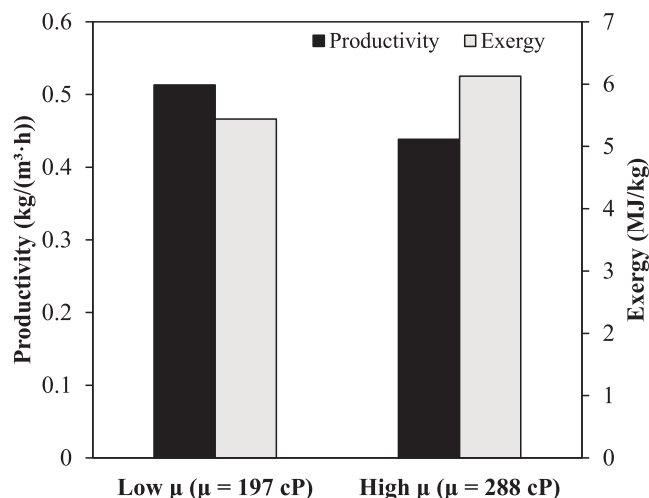
Fig. 13. Productivity and exergy depending on the $[P_{66614}][Im]$ viscosity for the minimum exergy point of $[P_{66614}][Im]$ Pareto chart. The viscosity value of 197 cP comes from $[P_{66614}][4\text{-}BrPyra]$ data, whereas 288cP relates to $[P_{2228}][4\text{-}BrIm]$.

capacity and mass transfer. Moving from liquid-sorbent to solid-sorbent processes by encapsulating or supporting the IL could be a promising alternative to overcome the kinetic limitations [56–58] and reduce the energy requirement of the regeneration step, in line with DAC literature of amino-based sorbents [26]. In this sense, Fig. 14 compares the cyclic capacities of the most promising AHA-ILs from this work ($[P_{66614}][3\text{-}BrPyra]$, $[P_{66614}][5\text{-}CH_3Im]$ and $[P_{66614}][Im]$) to those of solid adsorbents from preceding DAC studies [22]. All cases are calculated at equal sorption (see Table 1) and desorption conditions (0.1 bar and different desorption temperatures). It can be observed that the cyclic capacity trend of the selected AHA-ILs is comparable to Tri-PE-MCM-41 and Lewatit VP OC 106 adsorbents, but better than APDES-NFC from 370 K, achieving higher cyclic capacities than 0.41 mol/kg maximum (at 400 K) of this sorbent. In contrast, MIL-101(Cr)-PEI-800 sorbent shows remarkable values (0.2 – 0.-4 mol/kg) even at low desorption temperatures (345 – 360 K), but its cyclic capacity at 400 K (0.89 mol/kg) is quite similar to the rest of sorbents (0.75 mol/kg for Tri-PE-MCM-41 and 0.86 mol/kg for Lewatit VP OC 106) and the proposed ILs (0.67, 0.78, 0.82 mol/kg for $[P_{66614}][3\text{-}BrPyra]$, $[P_{66614}][Im]$ and $[P_{66614}][5\text{-}CH_3Im]$, respectively). In fact, the quantity of CO_2 captured per kg of IL could be enhanced by replacing the $[P_{66614}]$ cation with another cation with lower molecular weight as $[P_{2228}]$ [47]. Designing suitable AHA-
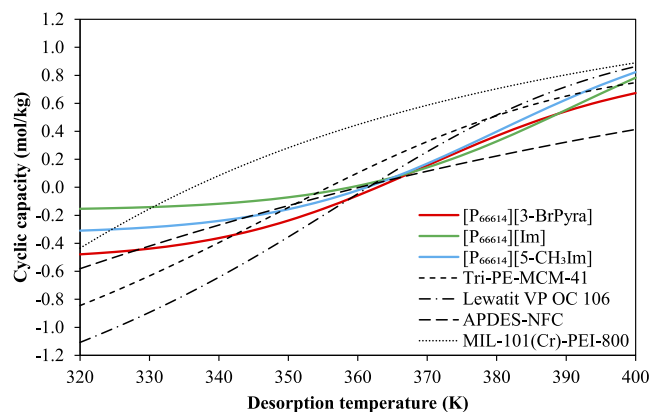
ILs for DAC application that meet the outstanding thermodynamics of solid sorbents when encapsulated or supported on a solid could be hence feasible, considering that some solid supports enable an IL nominal load up to 80 %weight [58].

Second, attention should be paid to highlight the role of water. Although the absorption capacity of AHA-ILs would not be negatively impacted by water [44], water adsorption is a crucial point of attention when considering solid supports, since it could affect the sorption of CO_2 depending on the ambient conditions and the solid characteristics [26]. Besides water isotherms, heat and mass transfer were previously identified to strongly determine the performance of different solid sorbents processes [22,26]. In fact, high specific mass transfer coefficients are particularly important for high productivity, which could be increased up to 10.6 kg/(m³·h) with minimal additional energy consumption as tabulated in Table 3 for solid sorbents.

According to the energy consumption reported in Table 4, DAC technologies based on the adsorbents represented in Fig. 14 exhibit particularly promising results compared to the solvent-based technologies presented in Table 3. MIL-101(Cr)-PEI-800 has the minimum energy demand (4.7 – 8.9 MJ/kg), significantly inferior than the best IL-based DAC absorption system (15.15 – 35.42 MJ/kg of $[P_{66614}][Im]$). Overall, enhancing the kinetics of absorption by encapsulating or supporting the proposed ILs is suggested to further improve their process performance [56–58] and bring the total cost of capture towards 100–200 $/ton_{CO2}$ [5,9,11].

5. Conclusions

In this work, 26 different ILs were molecular designed by a DFT/COSMO-RS method to study their feasibility to DAC processes. Suitable ILs for DAC purposes were detected by estimating the cyclic working capacity at DAC-relevant conditions from predicted CO_2 isotherms. $[P_{66614}][3\text{-}BrPyra]$, $[P_{66614}][5\text{-}CH_3Im]$ and $[P_{66614}][Im]$ exhibited promising cyclic capacity values comparable to those estimated for solid sorbents and up to 0.8 mol/kg. Detailed rate-based process modeling in Aspen Plus was used to simulate the DAC processes based on these ILs and the air contactor design from Carbon Engineering. A technical analysis was carried out to evaluate the ILs performance as chemical absorbents for DAC in terms of exergy, energy and productivity. Several design variables and operating conditions were assessed. Key findings of this analysis showed that: higher air velocity enhances the productivity at the expense of increasing the exergy demand; higher desorption temperature allows for greater desorption pressures and therefore lower exergy consumption; the IL inlet temperature on the air contactor has a negligible influence; the optimal mass flow coincides with the minimum exergy condition. The optimal operation was identified by range as Pareto front. Among the ILs evaluated, $[P_{66614}][Im]$ exhibited the most exergy (energy) efficient DAC process thanks to its greater cyclic capacity: 5.44(15.15) – 16.73(35.42) MJ/kg for a productivity range of 0.5 – 1.3 kg/(m³·h). Compared to other absorption technologies, its 5.44 MJ/kg minimum exergy is slightly lower than alkali (6.21 MJ/kg) and amine (5.59 MJ/kg) scrubbing references, but higher than those from solid sorbents. The IL viscosity was found to have substantial effects on the productivity, exergy and economics, worsening their values when it is increased. A simplified economic

Fig. 14. Cyclic capacity as function of the desorption temperature for the most promising ILs identified in this work and the solid sorbents from previous studies [22]. Adsorption conditions are: 293 K, 1 bar and 400 ppm of CO_2. Desorption vacuum pressure: 0.1 bar.

Table 4
Energy consumption of solid-based DAC technologies compared to the best IL of this work.

	Energy (MJ/kg)
MIL-101(Cr)-PEI-800	4.7 – 8.9 [22]
TRI-PE-MCM-41	6.8 [59]
APDES-NFC	9.7 – 11.4 [22]
Lewatit VPOC 106	10.7 – 13.1 [22]
$[P_{66614}]$ [Im]	15.51 – 35.42 (this work)

model allowed us to identify the trends and the major contributions to the total cost of the plant. Representative air contactor costs (2,000 – 50,000 $/m^3), and heat and electricity prices (0.01 – 0.1 $/kWh) were therefore considered. It was found that the total cost of the ILs-based DAC systems is drastically determined by the plant cost and the heat price. Costs maps are in line with other DAC solutions, which suggests IL-based approach could be a valid alternative to current commercialized DAC technologies. The kinetic advantage of solid-sorbent processes suggests that supported or encapsulated ILs might further enhance the performance of ILs (or compensate for higher viscosity values) taking benefit from their faster mass transfer kinetics to increment productivity without a significant extra energy penalty. Future work may address the application of these IL-based advanced materials and properly compare them to available solid sorbents.

Declaration of Competing Interest

The authors declare that they have no known competing financial interests or personal relationships that could have appeared to influence the work reported in this paper.

Data availability

Additional data not reported in Appendix A are available upon (email) request.

Acknowledgments

Appendix A. Supplementary data

Supplementary data to this article can be found online at https://doi.org/10.1016/j.cej.2023.143630.

References

[1] R. Hanna, A. Abdulla, Y. Xu, D.G. Victor, Emergency deployment of direct air capture as a response to the climate crisis, Nat. Commun. 12 (2021) 368.

[2] C. Breyer, M. Fasihi, C. Bajamundi, F. Creutzig, Direct air capture of CO_2: a key technology for ambitious climate change mitigation, Joule 3 (2019) 2053–2057.

[3] E.S. Sanz-Pérez, C.R. Murdock, S.A. Didas, C.W. Jones, Direct capture of CO_2 from ambient air, Chem. Rev. 116 (19) (2016) 11840–11876.

[4] C. Beuttler, L. Charles, J. Wurzbacher, The role of direct air capture in mitigation of anthropogenic greenhouse gas emissions, Frontiers in Climate 1 (2019).

[5] M. Ozkan, A. Zoelle, S. Homsy, H. Mantripragada, M. Woods, N. Roy, A. Kilstofte, M. Sturdivan, M. Steutermann, T. Fout, Current status and pillars of direct air capture technologies, iScience 25 (2022), 103990.

[6] IEA, Direct Air Capture 2022, IEA, Paris, 2022 https://www.iea.org/reports/direct-air-capture-2022.

[7] C. Drechsler, D.W. Agar, Intensified integrated direct air capture - power-to-gas process based on H_2O and CO_2 from ambient air, Appl. Energy 273 (2020), 115076.

[8] M. Fasihi, O. Efimova, C. Breyer, Techno-economic assessment of CO_2 direct air capture plants, J. Clean. Prod. 224 (2019) 957–980.

[9] G. Realmonte, L. Drouet, A. Gambhir, J. Glynn, A. Hawkes, A.C. Köberle, M. Tavoni, An inter-model assessment of the role of direct air capture in deep mitigation pathways, Nat. Commun. 10 (2019) 3277.

[10] J. Valentine, A. Zoelle, S. Homsy, H. Mantripragada, M. Woods, N. Roy, A. Kilstofte, M. Sturdivan, M. Steutermann, T. Fout, Direct Air Capture Case Studies: Sorbent System, United States, 2022, pp. Medium: ED.

[11] K.S. Lackner, H. Azarabadi, Buying down the Cost of Direct Air Capture, Ind. Eng. Chem. Res. 60 (22) (2021) 8196–8208.

[12] G. Holmes, D.W. Keith, An air–liquid contactor for large-scale capture of CO_2 from air, Philos. Trans. R. Soc. A Math. Phys. Eng. Sci. 370 (2012) 4380–4403.

[13] G. Holmes, K. Nold, T. Walsh, K. Heidel, M.A. Henderson, J. Ritchie, P. Klavins, A. Singh, D.W. Keith, Outdoor prototype results for direct atmospheric capture of carbon dioxide, Energy Procedia 37 (2013) 6079–6095.

[14] D.W. Keith, G. Holmes, D. St. Angelo, K. Heidel, A process for capturing CO_2 from the atmosphere, Joule 2 (8) (2018) 1573–1594.

[15] D.K. Howard Herzog, Affordable Direct Air Capture: Myth or Reality?, MIT Joint Program on the Science and Policy of Global Change (2022) https://globalchange.mit.edu/media/affordable-direct-air-capture-myth-or-reality.

[16] F. Sabatino, M. Mehta, A. Grimm, M. Gazzani, F. Gallucci, G.J. Kramer, M. van Sint Annaland, Evaluation of a direct air capture process combining wet scrubbing and bipolar membrane electrodialysis, Ind. Eng. Chem. Res. 59 (15) (2020) 7007–7020.

[17] F.M. Brethomé, N.J. Williams, C.A. Seipp, M.K. Kidder, R. Custelcean, Direct air capture of CO_2 via aqueous-phase absorption and crystalline-phase release using concentrated solar power, Nat. Energy 3 (2018) 553–559.

[18] R. Custelcean, N.J. Williams, K.A. Garrabrant, P. Agullo, F.M. Brethomé, H. J. Martin, M.K. Kidder, Direct air capture of CO_2 with aqueous amino acids and solid Bis-iminoguanidines (BIGs), Ind. Eng. Chem. Res. 58 (2019) 23338–23346.

[19] F. Barzagli, C. Giorgi, F. Mani, M. Peruzzini, Screening study of different amine-based solutions as sorbents for direct CO_2 capture from air, ACS Sustain. Chem. Eng. 8 (37) (2020) 14013–14021.

[20] S. Kikkawa, K. Amamoto, Y. Fujiki, J. Hirayama, G. Kato, H. Miura, T. Shishido, S. Yamazoe, Direct air capture of CO_2 using a liquid amine–solid carbamic acid phase-separation system using diamines bearing an aminocyclohexyl group, ACS Environmental Au (2022).

[21] A. Kiani, K. Jiang, P. Feron, Techno-economic assessment for CO_2 capture from air using a conventional liquid-based absorption process, Front. Energy Res. 8 (2020).

[22] F. Sabatino, A. Grimm, F. Gallucci, M. van Sint Annaland, G.J. Kramer, M. Gazzani, A comparative energy and costs assessment and optimization for direct air capture technologies, Joule 5 (8) (2021) 2047–2076.

[23] A. Goeppert, M. Czaun, G.K. Surya Prakash, G.A. Olah, Air as the renewable carbon source of the future: an overview of CO_2 capture from the atmosphere, Energ. Environ. Sci. 5 (2012) 7833–7853.

[24] S.A. Didas, S. Choi, W. Chaikittisilp, C.W. Jones, Amine-Oxide hybrid materials for CO_2 capture from ambient air, Acc. Chem. Res. 48 (10) (2015) 2680–2687.

[25] C. Gebald, J.A. Wurzbacher, P. Tingaut, A. Steinfeld, Stability of amine-functionalized cellulose during temperature-vacuum-swing cycling for CO_2 capture from air, Environ. Sci. Tech. 47 (17) (2013) 10063–10070.

[26] X. Zhu, W. Xie, J. Wu, Y. Miao, C. Xiang, C. Chen, B. Ge, Z. Gan, F. Yang, M. Zhang, D. O'Hare, J. Li, T. Ge, R. Wang, Recent advances in direct air capture by adsorption, Chem. Soc. Rev. 51 (15) (2022) 6574–6651.

[27] S. Deutz, A. Bardow, Life-cycle assessment of an industrial direct air capture process based on temperature–vacuum swing adsorption, NatureEnergy 6 (2021) 203–213.

[28] M.M.J. de Jonge, J. Daemen, J.M. Loriaux, Z.J.N. Steinmann, M.A.J. Huijbregts, Life cycle carbon efficiency of direct air capture systems with strong hydroxide sorbents, Int. J. Greenhouse Gas Control 80 (2019) 25–31.

[29] T. Terlouw, K. Treyer, C. Bauer, M. Mazzotti, Life cycle assessment of direct air carbon capture and storage with low-carbon energy sources, Environ. Sci. Tech. 55 (16) (2021) 11397–11411.

[30] A. Sinha, L.A. Darunte, C.W. Jones, M.J. Realff, Y. Kawajiri, Systems design and economic analysis of direct air capture of CO_2 through temperature vacuum swing adsorption using MIL-101(Cr)-PEI-800 and mmen-Mg2(dobpdc) MOF Adsorbents, Ind. Eng. Chem. Res. 56 (3) (2017) 750–764.

[31] H. Azarabadi, K.S. Lackner, A sorbent-focused techno-economic analysis of direct air capture, Appl. Energy 250 (2019) 959–975.

[32] T. Wang, C. Hou, K. Ge, K.S. Lackner, X. Shi, J. Liu, M. Fang, Z. Luo, Spontaneous cooling absorption of CO_2 by a polymeric ionic liquid for direct air capture, J. Phys. Chem. Lett. 8 (17) (2017) 3986–3990.

[33] E.A. Recker, M. Green, M. Soltani, D.H. Paull, G.J. McManus, J.H. Davis, A. Mirjafari, Direct air capture of CO_2 via ionic liquids derived from "waste" amino acids, ACS Sustain. Chem. Eng. 10 (36) (2022) 11885–11890.

[34] Z. Yang, S. Dai, Challenges in engineering the structure of ionic liquids towards direct air capture of CO_2, Green Chem. Eng. 2 (4) (2021) 342–345.

[35] M. Aghaie, N. Rezaei, S. Zendehboudi, A systematic review on CO_2 capture with ionic liquids: current status and future prospects, Renew. Sustain. Energy Rev. 96 (2018) 502–525.

[36] S. Zeng, X. Zhang, L. Bai, X. Zhang, H. Wang, J. Wang, D. Bao, M. Li, X. Liu, S. Zhang, Ionic-Liquid-Based CO_2 capture systems: structure, interaction and process, Chem. Rev. 117 (2017) 9625–9673.

[37] Q. Yang, Z. Wang, Z. Bao, Z. Zhang, Y. Yang, Q. Ren, H. Xing, S. Dai, New insights into CO_2 absorption mechanisms with amino-acid ionic liquids, ChemSusChem 9 (8) (2016) 806–812.

[38] B. Gurkan, B.F. Goodrich, E.M. Mindrup, L.E. Ficke, M. Massel, S. Seo, T.P. Senftle, H. Wu, M.F. Glaser, J.K. Shah, E.J. Maginn, J.F. Brennecke, W.F. Schneider, Molecular design of high capacity, low viscosity, chemically tunable ionic liquids for CO_2 capture, J. Phys. Chem. Lett. 1 (24) (2010) 3494–3499.

[39] S. Seo, M. Quiroz-Guzman, M.A. DeSilva, T.B. Lee, Y. Huang, B.F. Goodrich, W. F. Schneider, J.F. Brennecke, Chemically tunable ionic liquids with aprotic heterocyclic anion (AHA) for CO_2 capture, J. Phys. Chem. B 118 (21) (2014) 5740–5751.

[40] B.o. Hong, L.D. Simoni, J.E. Bennett, J.F. Brennecke, M.A. Stadtherr, Simultaneous process and material design for aprotic N-heterocyclic anion ionic liquids in postcombustion CO_2 capture, Ind. Eng. Chem. Res. 55 (30) (2016) 8432–8449.

[41] J. de Riva, V. Ferro, C. Moya, M.A. Stadtherr, J.F. Brennecke, J. Palomar, Aspen plus supported analysis of the post-combustion CO_2 capture by chemical absorption using the P-2228 CNPyr and P-66614 CNPyr AHA ionic liquids, Int. J. Greenhouse Gas Control 78 (2018) 94–102.

[42] D. Hospital-Benito, J. Lemus, C. Moya, R. Santiago, V.R. Ferro, J. Palomar, Techno-economic feasibility of ionic liquids-based CO_2 chemical capture processes, Chem. Eng. J. 407 (2021) 127196.

[43] D. Hospital-Benito, J. Lemus, C. Moya, R. Santiago, J. Palomar, Process analysis overview of ionic liquids on CO_2 chemical capture, Chem. Eng. J. 390 (2020), 124509.

[44] G.M. Avelar Bonilla, O. Morales-Collazo, J.F. Brennecke, Effect of water on CO_2 capture by aprotic heterocyclic anion (AHA) ionic liquids, ACS Sustain. Chem. Eng. 7 (19) (2019) 16858–16869.

[45] D. Hospital-Benito, J. Lemus, C. Moya, R. Santiago, J. Palomar, Improvement of CO_2 capture processes by tailoring the reaction enthalpy of Aprotic N-Heterocyclic anion-based ionic liquids, Chemical Engineering Journal Advances 10 (2022), 100291.

[46] C. Moya, D. Hospital-Benito, R. Santiago, J. Lemus, J. Palomar, Prediction of CO_2 chemical absorption isotherms for ionic liquid design by DFT/COSMO-RS calculations, Chemical Engineering Journal Advances 4 (2020), 100038.

[47] S. Seo, M.A. DeSilva, H. Xia, J.F. Brennecke, Effect of cation on physical properties and CO_2 solubility for phosphonium-based ionic liquids with 2-cyanopyrrolide anions, J. Phys. Chem. B 119 (35) (2015) 11807–11814.

[48] V.R. Ferro, C. Moya, D. Moreno, R. Santiago, J. de Riva, G. Pedrosa, M. Larriba, I. Diaz, J. Palomar, Enterprise ionic liquids database (ILUAM) for Use in Aspen ONE programs suite with COSMO-based property methods, Ind. Eng. Chem. Res. 57 (3) (2018) 980–989.

[49] S.-T. Lin, S.I. Sandler, A priori phase equilibrium prediction from a segment contribution solvation model, Ind. Eng. Chem. Res. 41 (5) (2002) 899–913.

[50] J. de Riva, J. Suarez-Reyes, D. Moreno, I. Diaz, V. Ferro, J. Palomar, Ionic liquids for post-combustion CO_2 capture by physical absorption: thermodynamic, kinetic and process analysis, Int. J. Greenhouse Gas Control 61 (2017) 61–70.

[51] G.D. Ulrich, P.T. Vasudevan, Chemical Engineering Process Design and Economics: A Practical Guide, Process Pub.2004.

[52] D. Hospital-Benito, J. Lemus, C. Moya, R. Santiago, C. Paramio, J. Palomar, Aspen plus supported design of pre-combustion CO_2 capture processes based on ionic liquids, Sep. Purif. Technol. 290 (2022), 120841.

[53] R. Socolow, M. Desmond, R. Aines, J. Blackstock, O. Bolland, T. Kaarsberg, N. Lewis, M. Mazzotti, A. Pfeffer, K. Sawyer, Direct air capture of CO_2 with chemicals: a technology assessment for the APS panel on public affairs, American Physical Society, 2011.

[54] A.N. Keller, C.L. Bentley, O. Morales-Collazo, J.F. Brennecke, Design and characterization of aprotic N-heterocyclic anion ionic liquids for carbon capture, J. Chem. Eng. Data 67 (2) (2022) 375–384.

[55] J. Palomar, M. Larriba, J. Lemus, D. Moreno, R. Santiago, C. Moya, J. de Riva, G. Pedrosa, Demonstrating the key role of kinetics over thermodynamics in the selection of ionic liquids for CO_2 physical absorption, Sep. Purif. Technol. 213 (2019) 578–586.

[56] C. Moya, N. Alonso-Morales, J. de Riva, O. Morales-Collazo, J.F. Brennecke, J. Palomar, Encapsulation of ionic liquids with an aprotic heterocyclic anion (AHA-IL) for CO_2 capture: preserving the favorable thermodynamics and enhancing the kinetics of absorption, J. Phys. Chem. B 122 (2018) 2616–2626.

[57] T. Song, G.M. Avelar Bonilla, O. Morales-Collazo, M.J. Lubben, J.F. Brennecke, Recyclability of encapsulated ionic liquids for post-combustion CO_2 capture, Ind. Eng. Chem. Res. 58 (12) (2019) 4997–5007.

[58] R. Santiago, J. Lemus, D. Moreno, C. Moya, M. Larriba, N. Alonso-Morales, M. A. Gilarranz, J.J. Rodriguez, J. Palomar, From kinetics to equilibrium control in CO_2 capture columns using encapsulated ionic liquids (ENILs), Chem. Eng. J. 348 (2018) 661–668.

[59] A.R. Kulkarni, D.S. Sholl, Analysis of equilibrium-based TSA processes for direct capture of CO_2 from air, Ind. Eng. Chem. Res. 51 (25) (2012) 8631–8645.